minerals

MDPI

Article

Chemical and Mineralogical Characterization of Waste from Abandoned Copper and Manganese Mines in the Iberian Pyrite Belt, Portugal: A First Step Towards the Waste-to-Value Recycling Process

Daniel P. S. de Oliveira [1,2,*], Teresa P. Silva [1], Igor Morais [3] and João A. E. Fernandes [1]

[1] Mineral Resources and Geophysics Research Unit, Laboratório Nacional de Energia e Geologia (LNEG), Estrada da Portela, Bairro do Zambujal—Alfragide, Apartado 7586, 2610-999 Amadora, Portugal; teresa.pena@lneg.pt (T.P.S.); joao.fernandes@lneg.pt (J.A.E.F.)
[2] Mineral Resources Expert Group, EuroGeoSurveys, Rue Joseph II, 36–38, 1000 Brussels, Belgium
[3] Mineral Resources and Geophysics Research Unit, Laboratório Nacional de Energia e Geologia (LNEG), Bairro da Vale d'Oca, Apartado 14, 7601-909 Aljustrel, Portugal; igor.morais@lneg.pt
* Correspondence: daniel.oliveira@lneg.pt

Abstract: This study examines the chemical and mineralogical composition of waste materials from abandoned copper and manganese mines in the Iberian Pyrite Belt, Portugal, as a first step toward their potential recycling for critical and strategic raw materials (CRM and SRM). Using portable X-ray fluorescence (pXRF) and other analytical techniques, this research highlights the presence of valuable elements, including copper, manganese, and rare earth elements, in concentrations significantly above their crustal abundance. The findings underscore the dual potential of these wastes: as sources of secondary raw materials and for mitigating environmental hazards such as acid mine drainage (AMD). Recovered materials include chalcopyrite, pyrolusite, and rhodochrosite, with critical elements like cobalt, lithium, and tungsten identified. pXRF proved to be a reliable, cost-effective tool for rapid field and laboratory analyses, demonstrating high precision and good correlation with standard laboratory methods. The study emphasizes the importance of characterizing historical mining waste to support a circular economy, reduce reliance on foreign material imports, and address environmental challenges. This approach aligns with the European Union's Critical Raw Materials Act, promoting sustainable resource use and the recovery of strategic resources from historical mining sites.

Keywords: mineralogical composition; mining waste; historical mines; critical raw materials; strategic raw materials; circular economy

Academic Editor: Carlos Sierra Fernández

Received: 26 November 2024
Revised: 20 December 2024
Accepted: 3 January 2025
Published: 7 January 2025

Citation: de Oliveira, D.P.S.; Silva, T.P.; Morais, I.; Fernandes, J.A.E. Chemical and Mineralogical Characterization of Waste from Abandoned Copper and Manganese Mines in the Iberian Pyrite Belt, Portugal: A First Step Towards the Waste-to-Value Recycling Process. *Minerals* **2025**, *15*, 58. https://doi.org/10.3390/min15010058

1. Introduction

The EU's concerns about the sourcing and supply of raw materials are more worrisome today than ever. The initial calls for action in this area date back to the Council's 2nd Environment Action Programme, which highlighted the Community's reliance on raw materials sourced from outside its borders [1]. More than two decades later, the European Commission launched the Raw Materials Initiative, the first integrated strategy focused on enhancing access to these resources [2]. This initiative led to the creation of the first list of critical raw materials (CRM).

By definition, a CRM is a material that is both economically important and has a high supply risk and lack of viable substitutes while a strategic raw material (SRM) is a

natural resource or material that is crucial for a nation's economic stability, technological development, or national security. Unlike critical raw materials, which are assessed based on economic importance and supply risk, strategic raw materials are defined by their role in fulfilling long-term strategic goals, such as energy independence, military capability, or technological leadership.

Since then, the importance of securing access to raw materials has been reinforced through various high-level EU strategies [3]. However, recent disruptions in supply chains caused by the COVID-19 pandemic and the ongoing conflict in Ukraine have introduced additional complexities to this challenge [4,5]. On 16 March 2023, the European Commission introduced the Critical Raw Materials Act (CRMA) as part of its wider "Green Industrial Plan" and alongside the "Net-Zero Industry Act" (NZIA). According to the European Commission [3], the initiative aims to reduce the EU's reliance on CRM while promoting a sustainable and competitive landscape for CRM value chains within the EU [6]. The search for primary critical and strategic raw materials (CRM and SRM, respectively), and even secondary raw materials, is a major concern nowadays given their high consumption [6–8]. One way to minimise the stress on new mining targets definition and primary mineral extraction is to search for these materials in the tailings of historical mines, which have resulted from the milling of the bulk ore-bearing rock or even from mineral processing (e.g., slag) [9]. Mining waste recycling also helps to prevent acid mine drainage (AMD). Thus, the reprocessing of mining waste provides, beyond the extraction of primary critical and secondary raw materials, the removal of hazardous substances and a new opportunity to manage the remaining waste in historical mining sites.

There are several examples in the literature: (a) several authors claim that copper mine drainage (CMD) generated from copper mining and smelting is a type of AMD, with a high sulphate concentration and large amounts of metal ions such as Fe, Cu, and Mn, e.g., [10]; moreover, these authors proposed a combined process including Fe, Cu, and S pretreatment recovery units through chemical oxidation and the sulphur biocycling of CMD materials; and (b) a copper recuperation plant at the gold mine Pueblo Viejo, in the Dominican Republic, using sulfidogenic microorganisms to remediate metal waste [11].

Equally important in recent years, manganese recovery from waste using the bio-oleaching of metal using microbes has provided advantages over the traditional method of recovery [12]. The Chvaletice Manganese Project (https://www.mn25.ca/chvaletice-manganese-project, accessed on 10 December 2024) in Czechia is an example of recycling and remediation by reprocessing old tailings from a decommissioned mine to produce battery-grade manganese products for the electric vehicle industry [13].

Mixtures of synthetic tetrahedrite samples and tetrahedrite–tennantite ore samples from abandoned Barrigão mine dumps located in the Portuguese zone of the Iberian Pyrite Belt (IPB) have been produced by solid-state mechanochemical synthesis to explore their use in tellurium-free thermoelectric (TE) materials [14], for application in heavy and maritime industries, and also as primary power sources for off-grid sensors and IoT devices (START project, https://www.start-heproject.com/, accessed on accessed on 10 December 2024).

The aim of this study is to characterize the chemical and mineralogical waste from historical Cu and Mn mine sites in view of the first evaluation of their potential for recycling CRM, SRM, and other valuable elements. The performance of the portable equipment used to carry out the chemical characterization in these complex samples is also assessed on the wastes/tailings/slags from abandoned Cu and Mn exploitations in the Portuguese sector of the IPB.

1.1. Historical Mines Overview

Portugal is one of the European countries with the longest and strongest mining traditions, given the richness of the Iberian Peninsula in mineral resources and the favorable conditions for mineral deposits discovery, e.g., [15].

In the south of the country, there are two large tectonostratigraphic zones that contain a wide variety of mineral deposits. The Ossa Morena Zone (OMZ) to the north is the Iberian Massif geotectonic unit that displays the greatest variety of types of mineralization as well as the largest number of ore deposits and showings (>650). It includes a wide range of commodities such as iron, lead-zinc, copper, gold, silver, antimony, nickel, manganese, tungsten, mercury, barite, variscite, uranium, and coal [16]. The South Portuguese Zone (SPZ) is the southernmost of the zones in the Iberian Massif and includes the Iberian Pyrite Belt (IPB), one of the largest districts of volcanogenic massive sulphide (VMS) deposits in the world, and is a critical source of base metals (Cu, Pb, and Zn) for Europe. Confirmed resources exceed 1700 Mt of massive sulphides with grades of around 1.2% Cu, 1% Pb, and 3% Zn, as well as more than 300 Mt of stockwork-type copper mineralization [17].

For this study, several old mines have been selected—one in the Ossa Morena Zone (Aparis mine) and ten in the South Portuguese Zone (Lousal, Brancanes, Barrigão, Porteirinhos, Algaré, Cova dos Mouros, Ferragudo, Ferrarias e Castelo, Cerro do Serpe, and Balança—representing several types of ore deposits (VMS, copper veins, and manganese lenses) (Figure 1).

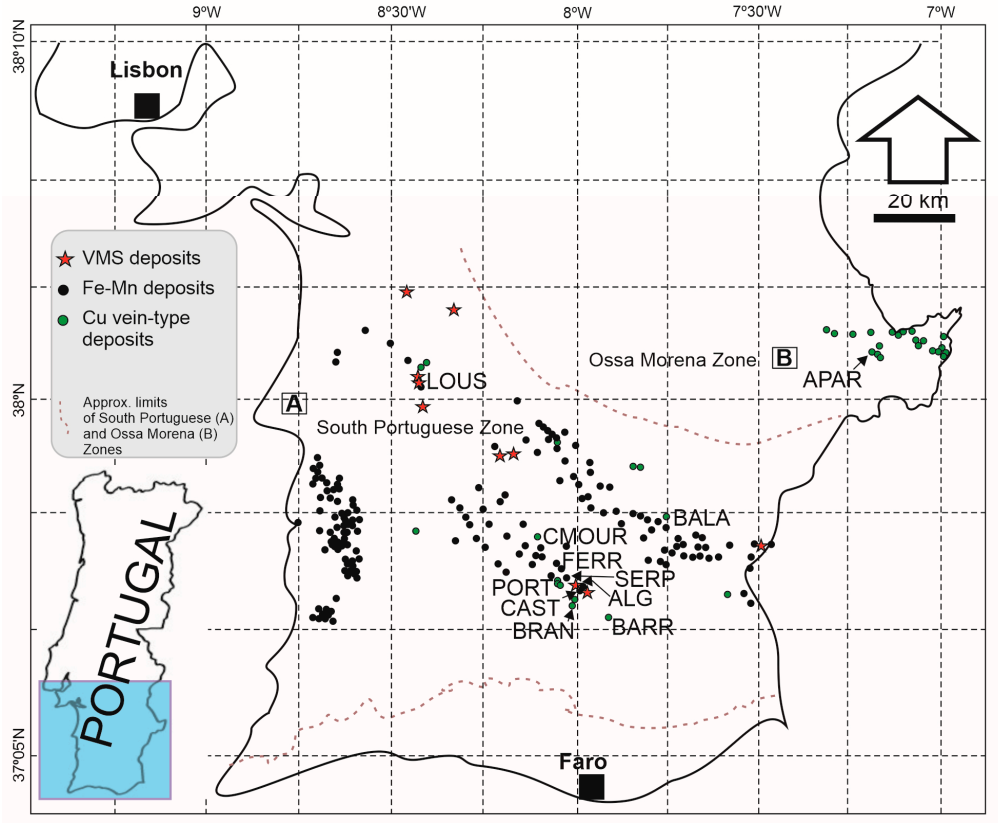

Figure 1. Simplified map of the studied areas with the approximate location of several old mines. (**A**) Iberian Pyrite Belt sector in the South Portuguese Zone; (**B**) Barrancos sector in the Ossa-Morena Zone. Mine name abbreviations: LOUS—Lousal; BALA—Balança; CMOUR—Cova dos Mouros—Castro Verde; FERR—Ferragudo; SERP—Cerro do Serpe; PORT—Porteirinhos; CAST—Ferrarias e Castelo; ALG—Algaré; BRAN—Brancanes; BARR—Barrigão; APAR—Aparis (see references [18,19] for geological information).

1.1.1. VMS-Type Deposits

The Lousal Mine is an old pyrite (FeS_2) mine located in the NW sector of the IPB, approximately 120 SSE of Lisbon (Figure 1A), in a complex structure formed by the volcano–sedimentary complex (VSC) (Famennian to Visean age) and the Phyllite–Quartzite Group (PQG) (Givetian to latest Famennian age—Strunian Biozone), the two lithostratigraphic units of the IPB. Opened in 1900 and closed in 1988, the subvertical deposit was exploited by galleries to a ~500 m depth with an NW direction. It is a VMS hosted in an antiform structure.

1.1.2. Cu Vein-Type Deposits

Late-Variscan hydrothermal copper sulphide veins systems occur in the OMZ and SPZ. The old Aparis Mine located in the Barrancos area (OMZ; Figure 1B) is an ore system associated with N10 E to N20 E subvertical veins (>2000 m extension) and mined up to a 150 m depth. The mineralogy is composed of chalcopyrite + pyrite ± marcasite ± pyrrhotite ± galena ± tetrahedrite ± arsenopyrite + quartz + dolomite + ankerite ± siderite ± calcite ± chlorite [20].

Along the IPB, dozens of Cu-bearing veins associated with fault breccias were exploited in the 19th century for copper, lead, zinc, barium, and antimony. Some of the copper veins are aligned along the Neves-Corvo copper trend indicating a possible remobilization of metals at depth. One such mine, the Barrigão Mine, consists of two converging metric-thick vein structures, extending approximately 1800 m along strike [21,22] SSE of the Neves-Corvo Mine (Figure 1A). The Barrigão copper ore is represented by fault breccias composed of chalcopyrite, tennantite, tetrahedrite, and pyrite, with minor or rare arsenopyrite, löllingite, sphalerite, and native bismuth and an undetermined Cu–Sn–Ge-sulphide in a matrix of quartz, angular fragments of black shale, and carbonate minerals [23].

Another type of such a deposit, the Brancanes Mine, is located close to the Neves-Corvo mine (approximately 3 km to the WSW; Figure 1A). The Brancanes Copper Mining Company initiated mining activity in 1883, exploiting a copper vein with an N45° W, 50° E orientation rich in chalcopyrite and pyrite with quartz and carbonates [24]. The quartz + carbonate + sulphide veins are installed in shales and greywackes of the Mértola Formation. The superficial levels of copper mineralization were largely represented by malachite and more rarely by azurite and covellite.

The Porteirinhos deposit (Figure 1A) resulted in a small old mine composed of a 1.2 m thick Cu-bearing quartz vein with an N70° E orientation in the Mértola Formation. The mineralogy is characterized by chalcopyrite + arsenopyrite + pyrite and azurite, with malachite and tetrahedrite as secondary minerals.

The Algaré Mine is located very close to the Neves-Corvo mine next to the Neves-Corvo thrust (Figure 1A). The structure is characterized by fractures with an orientation of NW-SE and 70° NE and runs sub-parallel to the regional structure. The massive pyrite has an average content of 0.45% of copper and the mineralogy is composed of pyrite + chalcopyrite + arsenopyrite and azurite, stannite, galena, and malachite.

The Cova dos Mouros Mine is located 1 km W of the village of Castro Verde (Figure 1A). The structure corresponds to a gossan (likely a copper vein or VMS deposit) anomalous in base metals. The region was previously investigated by "Serviço de Fomento Mineiro" (currently LNEG).

1.1.3. Manganese Lens-Type Deposits

The manganese deposits in the IPB have been mined throughout history. These are related to chert and jasper horizons and occur at a stratigraphic position roughly similar to that of massive sulphide lenses [25] and Upper Volcano-Sedimentary Complex se-

quences [26,27]. Their size and metal content make them uneconomic nowadays, although they were important in the past [28].

The most important Fe-Mn in the Portuguese sector of the IPB are the Ferragudo and Balança mines (Figure 1A). The Ferragudo Mine is a stratiform mineralized structure (50° NW, 45° NE) composed of lenses of oxides, carbonates, and silicates of Mn and Fe (several bodies with thicknesses varying from 1 to 12 m over an extension of approximately 150 m). Mineralization is associated with the lithologies of the Volcano-Sedimentary Complex. The main ore was composed of pyrolusite, psilomelane, wad, rhodochrosite, rhodonite, manganite, and hematite, occurring in quartz gangue + carbonates [29–31]. The Balança Mine with a 60° NW, 80° NE direction is very similar to the Ferragudo mine. The paragenetic mineral assemblage is composed of pyrolusite, psilomelane, wad, rhodochrosite, rhodonite, manganite, hematite, and quartz in a quartz and carbonate gangue.

Ferrarias e Castelo and Cerro do Serpe are small manganese mines that had very incipient exploitation at the beginning of the 20th century. Exploitation was essentially carried out in open pits and small shafts and galleries. The mineralization corresponds to small lenticles of manganese oxides (essentially pyrolusite) and is associated with jasper and chert horizons of the Upper Vulcano-Sedimentary Complex.

2. Materials and Methods

2.1. Sampling

A total of 45 samples were collected in the different types of mine wastes and deposit types (see the description of the samples in Table 1). The variations included coarse-, medium-, and fine-grained types and depended on the sample type (Figure 2). The sample type reflects the processing methods that were carried out in each mining area.

At each sampling location, four individual samples were combined to create a composite sample representative of the mine waste at that site.

The total sample collected was between 5 and 6 kg at a depth of 30–40 cm depending on the morphology of the waste.

In the lab, the samples for chemical and mineralogical analyses were initially dried at 35 °C for 3 weeks. Coarse grain samples were previously cut into small portions with a diamond saw.

The samples were initially crushed using a tungsten jaw crusher (Retsch BB250 XL), and a 200 g split was processed using a secondary crusher (Retsch BB50 with tungsten jaws), reducing the particle size to below 500 µm. The material was then sieved through a 75 µm mesh to separate the particles already at the desired grain size for chemical analysis, ensuring proper calibration for further processing in the agate mill (Retsch RS200). After pulverization in the agate mill, the sample was sieved again through a 75 µm mesh to confirm that the particle size was uniformly calibrated.

Table 1. Description of collected samples (sample reference was simplified). Material size: C—Coarse-grained (>0.5 to 1 mm); M—Medium-grained (>0.25 to 0.5 mm); F—Fine-grained (<0.25 mm). Sample type (represent the type of material of mining waste): Processing—Mining waste product of some type of mechanical treatment (example: float plant; manual selection); Dump composite—Mining wastes composed of host rocks with heterogeneous amounts of ore.

Sample Reference	Mine Name	Geotectonic Zone	Mine Type	Material Size	Sample Type	Sample Description
LOUS/001	Lousal	South Portuguese Zone—Iberian Pyrite Belt	VMS	M	Processing	Crushed ore (mainly pyrite) with clasts of quartz. Oxidation cap with 5 cm
LOUS/002				C	Dump composite	Blocks of mineralization host rocks (felsic volcanic rocks, shales, and quartz)
LOUS/003				F	Processing	Tailings inside the acid lagoons. Material very fine, composed of neoformation minerals
LOUS/004				C	Dump composite	Blocks of mineralization host rocks (essentially shales)
LOUS/006				C	Dump composite	Blocks of mineralization host rocks (essentially shales). Occasionally massive pyrite blocks
LOUS/007				C	Dump composite	Blocks of mineralization host rocks (essentially shales and volcanic rocks). Occasionally massive pyrite blocks. Neoformation minerals
LOUS/008				F	Processing	Tailings inside the acid lagoons. Material very fine, composed of neoformation minerals
LOUS/009				M	Processing	Crushed pyrite with blocks of host rocks (volcanic rocks and shales). Neoformation minerals (sulfates)
LOUS/010				C	Processing	Shales with fine pyrite associated. Quartz and neoformation minerals
LOUS/011				C	Dump composite	Shales with pyrite blocks. Neoformation minerals
LOUS/012				C	Dump composite	Pyrite blocks with rare volcanic rocks and quartz. Neoformation minerals
LOUS/013				C	Dump composite	Shales with pyrite blocks
LOUS/014				C	Processing	Crushed pyrite

Table 1. *Cont.*

Sample Reference	Mine Name	Geotectonic Zone	Mine Type	Material Size	Sample Type	Sample Description
PORT/001	Porteirinhos	South Portuguese Zone—Iberian Pyrite Belt	Cu veins	C	Dump composite	Shales and graywackes with blocks of quartz (pyrite, chalcopyrite, and malachite
PORT/001 Ore				C	Ore	Quartz with primary sulfides
BARR/001	Barrigão			C	Dump composite	Shales and graywackes with fine material composed of host rock crushed and cooper neoformation minerals
BARR/002				C	Roasting	Slags probably from 19th century. Blocks of coal are observed
BARR/003				C	Ore	Ore blocks with host rocks associated
ALG/001	Algaré			M	Dump composite	Crushed pyrite with clast of host rocks
Algaré Ore				C	Ore	Massive pyrite
ALG/002				M	Dump composite	Host rocks (shales and volcanic rocks) with neoformation minerals (malachite)
ALG/003				C	Processing	Blocks of volcanic rocks, shales, and quartzites with oxidized sulfides
ALG/004				C	Dump composite	Quartzites and volcanic rocks with iron and manganese oxides
ALG/004 Ore				C	Dump composite	Iron and manganese oxides
BRAN/001	Brancanes			M	Roasting	Slags probably from 19th century. Blocks of coal are observed
BRAN/002				F	Processing	Post flotation tailings
BRAN/003				M	Roasting	Slags probably from 19th century. Blocks of host rocks
Brancanes Ore				C	Ore	Quartz and carbonate veins with sulfides (chalcopyrite, tetrahedrite)
CMOUR/001 Ore	Cova dos Mouros			C	Dump composite	Volcanic rocks, quartz, and cherts with Fe and Mn concretions

Table 1. *Cont.*

Sample Reference	Mine Name	Geotectonic Zone	Mine Type	Material Size	Sample Type	Sample Description
APAR/001	Aparis	Ossa Morena Zone	Cu veins	C	Dump composite	Quartz blocks and host rocks (shales). Copper neoformation minerals
APAR/002				C	Dump composite	Quartz blocks and shales. Sulfides impregnation in the quartz
APAR/003				C	Dump composite	Quartz blocks with copper neoformation minerals
APAR/004				F	Processing	Post flotation tailings
APAR/005				F	Processing	Post flotation tailings
APAR/006				F	Processing	Post flotation tailings
APAR/007				F	Processing	Post flotation tailings
FERR/001	Ferragudo	South Portuguese Zone—Iberian Pyrite Belt	Fe-Mn lens	M	Processing	Crushed material composed of iron and manganese oxides
FERR/002				F	Processing	Black material composed of crushed ore
FERR/003				C	Dump composite	Blocks of host rocks (shales) and cherts with Fe and Mn impregnation
FERR/004				M	Processing	Black material composed of crushed ore
CAST/001	Ferrarias and Castelo			C	Dump composite	Jaspers and cherts with iron and manganese mineralization. Pyrite associated with chert facies
CAST/002				C	Dump composite	Iron and manganese oxides with pyrite
CAST/003				C	Dump composite	Jaspers and cherts with iron and manganese mineralization. Pyrite associated with chert facies
CAST/004				C	Dump composite	Shales with iron and manganese impregnation
SERP/001 Ore	Serpe			C	Dump composite	Jaspers and cherts block with iron and manganese mineralization
BALA/001	Balança			C	Dump composite	Jaspers and cherts block with iron and manganese mineralization

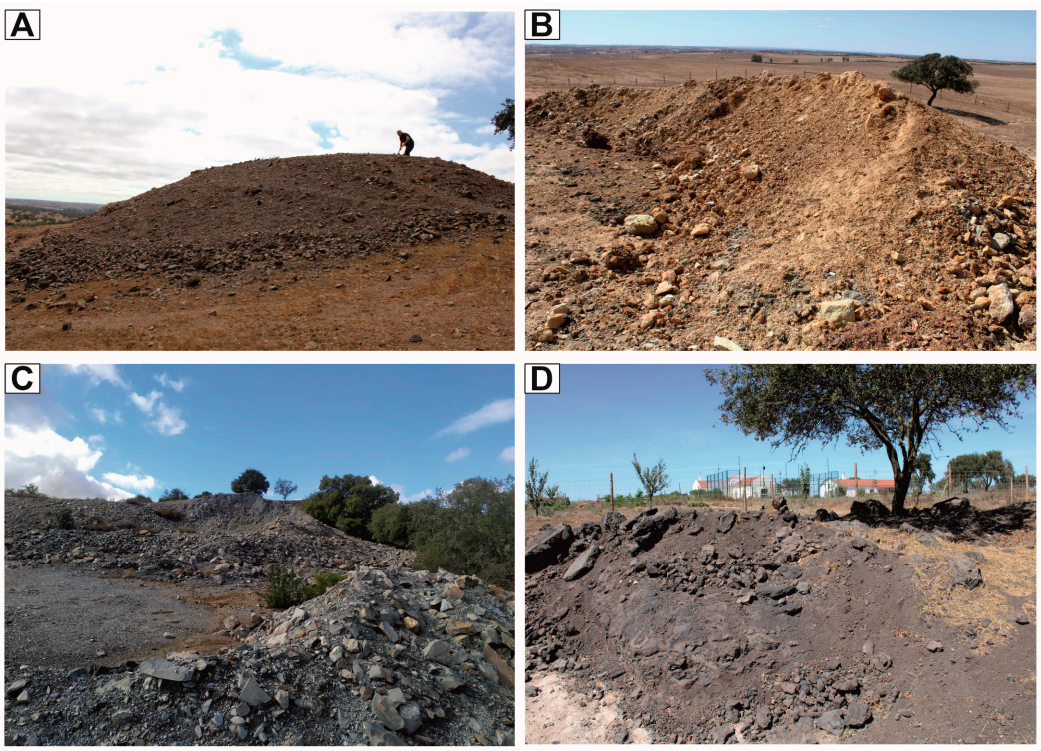

Figure 2. General aspects of mine dump waste in selected mines. (**A**) Mine wastes of Algaré Cu vein deposit; (**B**) Gossan/alteration zone in the Cova dos Mouros—Castro Verde occurrence; (**C**) aspect of mine wastes with high sulphide content (Ge and Sb) in the Barrigão Cu deposit; (**D**) final manganese concentrate (manganese oxides) in the Ferragudo iron-manganese deposit.

2.2. Methodology

Portable X-ray fluorescence (pXRF) equipment, X-MET8000 Expert Geo from HITACHI (Tokyo, Japan), was used for rapid chemical analysis of the powdered samples in the laboratory using a benchtop stand. This apparatus was equipped with a Rh tube (4 W) and a silicon drift detector (SDD). Two analytical programs (calibrations) were used: mining (40 kV, 120 s per sample) and REE (for the rare earth elements, during 180 s, 50 kV).

A multi-analytic approach was used to ensure that the pXRF equipment could be used with confidence in the determination of the elemental composition of waste materials. With this purpose, the results of selected samples were compared with chemical analyses obtained by XRF (wavelength dispersive, WDS) laboratory equipment (Philips PW2404, Andover, MA, USA). It was not possible to obtain fused discs, so the analyses of waste samples were carried out on pressed pellets. The major elements were obtained with a semi-quantitative program and the minor and trace with the "Protrace" program.

Major and trace elements of selected samples were also analysed by Activation Laboratories (ACTLABS, Ancaster, ON, Canada) using analytical package UT-3—inductively coupled plasma mass spectroscopy (ICP-MS) analyses by 4-acid (hydrochloric, nitric, perchloric, and hydrofluoric) digestion and by instrumental neutron activation analysis (INAA). Quality control was ensured by internal protocols at the laboratory (see www.actlabs.com (accessed on 10 December 2024) and Supplementary Materials, Table S1, folder QC-ACTLABS).

Powder X-ray diffraction (XRD) data were collected using a D8 Advance Bruker AXS diffractometer (Bruker AXS GmbH, Karlsruhe, Germany) with Cu Kα radiation, operating at 40 kV and 40 mA. The powder diffractograms (5–70° 2θ) were obtained using a step size of 0.015° and a step time of 0.3 s with a LYNXEYE XE-T detector. The XRD data treatment was performed using DIFFRAC.EVA v5 software for phase identification.

3. Results and Discussion

A raw comparison between methodologies concerning chemical characterisation was performed first. Indeed, pXRF is a useful tool for a quick and inexpensive overview (both in the field and in the laboratory) of the range of elements that a waste sample can contain, e.g., [32]. No significant difference in the element concentration was observed between performing one or an average of three measures collected at different points/areas of the same sample, indicating good precision of the equipment. Some examples can be seen in Figure 3. The complete table and all graphics ordered alphabetically are supplied as Supplementary Materials in Table S1.

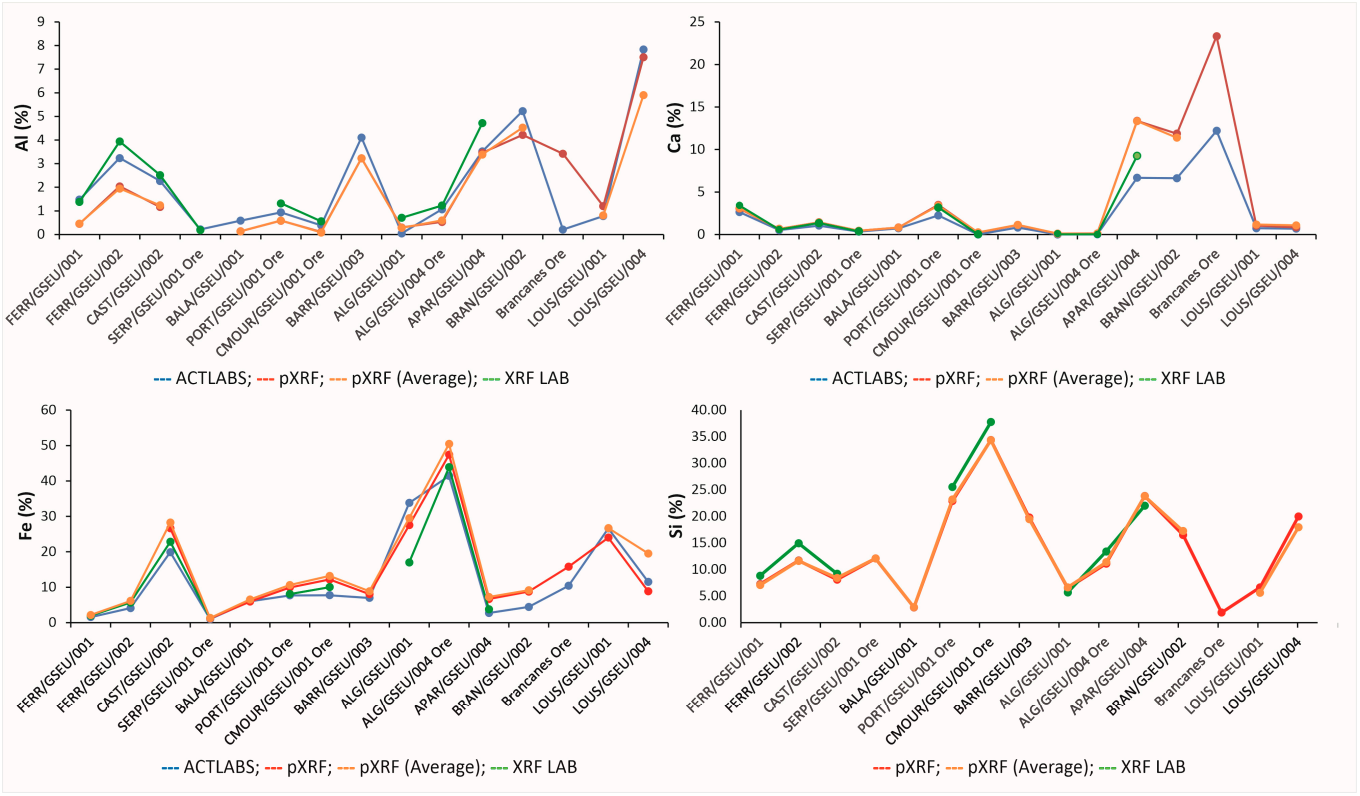

Figure 3. Comparison between the chemical results (Al, Fe, and Ca) obtained in ACTLABS, with pXRF (one measure and average of three measures) and XRF laboratory equipment. Si was only obtained through pXRF and XRF laboratory equipment.

The accuracy of pXRF equipment was tested through a comparison with measures obtained for selected samples in a certified international laboratory (ACTLABS) and with XRF laboratory equipment (WDS), as previously mentioned. An evaluation with international standards was also performed, but as the concentrations of many elements were not known, the methodology described was adopted. The correlation between ACTLABS and pXRF equipment (Table S1) produced good values for Al, As, Ba, Ca, Cu, Fe, Ga, K, Mg, Mn, Mo, Ni, Pb, Rb, S, Sb, Se, Sr, Ti, Zn, and W ($R^2 \geq 0.7$). Despite the strong correlation, the line slopes often deviate from the unity. A slope higher than 1 is assigned to Cu, Rb, Ni, As, K, Mn, Sr, Ca, Pb, Se, W, Mo, S, Zn, and Sb (ordered from largest to smallest). For Ti, the slope is approximately 1, as well as for Si (correlation between pXRF and XRF LAB as ACTLABS did not analyze Si). A slope of less than 1 was observed for Fe, Al, Ga, Ba, and Mg (examples in Figure 4). The lowest reliability measurements ($R^2 < 0.7$) were observed for Ag, Bi, Cd, Co, Cr, Hf, Hg, Nb, P, Sc, Sn, Ta, Th, U, V, Y, and Zr, plus La, Ce, Pr, and Nd (the rare earth analytical program should be revised). The graphic of ACTLABS vs. XRF laboratory shows, for almost all the elements mentioned above with $R^2 \geq 0.7$, slopes closer

to 1. However, given the high content of some elements (e.g., Sr, Ba, Sn, Cu, Pb, and As) in some samples, a semi-quantitative analysis program was used in these specific cases. On the other hand, the high content of various elements (e.g., Cu, Pb, S, As, Mn, and Sr) in some samples exceeded the maximum detection limit of the analytical program used in ACTLABS.

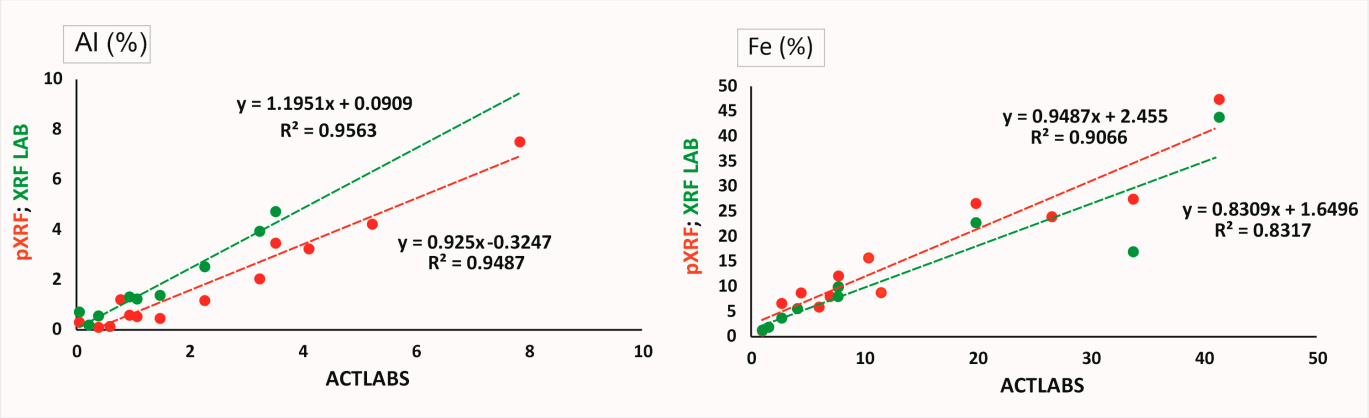

Figure 4. Examples of correlations obtained between chemical analyses: ACTLABS vs. pXRF and ACTLABS vs. XRF laboratory equipment.

The great discrepancy in elemental concentrations due to the complexity of the samples makes it difficult to choose the best analytical method to use. However, for a first step toward a more structured study, the pXRF equipment gave quick and acceptable results for many elements.

The complete table of chemical analyses performed on wastes from copper and manganese abandoned mines is presented in Supplementary Materials, Table S2, where the major contents of each element are assigned, bearing in mind the limitations of the techniques and the correlations/slope obtained (see Table S1). For example, Cu exceeds the maximum detection limit of the analytical program used in ACTLABS; conversely, the semi-quantitative analysis program was used with XRF laboratory equipment instead of the quantitative program; therefore, the pXRF results were considered in this case. Concerning Mo, the correlation between the ACTLABS and pXRF results is high (R^2 = 0.9913) but the slope is slightly higher than 1 (1.3), so the data from the international laboratory were chosen. In general, samples taken from the old copper mines show higher values of Ag (72 ppm), Al (12%), As (8.4%), Au (1110 ppb), Bi (217 ppm), Ca (12%), Co (209 ppm), Cu (27.5%), Fe (47.4%), Ge (9.6 ppm), Hf (9.6 ppm), Hg (106 ppm), In (6 ppm), K (3.3%), Li (83 ppm), Mg (6.6%), Ni (750 ppm), Pb (3%), Rb (132 ppm), S (38%), Sb (665 ppm), Sc (19 ppm), Se (132 ppm), Si (37.8%), Sn (139 ppm), Th (14.9 ppm), Zn (0.2%), Zr (271 ppm), and REE (La—47.6 ppm, Ce—94.7, Pr—11.3, Nd—42.1, Sm—7.4, Eu—1.28, Gd—5.1, Dy—4.1, Tb—0.7, Ho—1.2, Er—4.3, Tm—0.8, Yb—6, and Lu—1 ppm). Conversely, the waste from manganese mines is richer in Ba (1.5%), Be (7 ppm), Cr (111 ppm), Ga (129 ppm), Mn (38.6%), Mo (205 ppm), Sr (0.4%), Tl (94.4 ppm), V (170 ppm), and W (790 ppm). Cd, Cs, Na, Nb, P, Re, Ta, Tb, Te, Ti, U, and Y are random.

Many of these elements are considered critical and/or strategic raw materials [7]: CRM: As, Be, Bi, Co, Ga, Ge, Hf, HREEs (heavy rare earth elements—Dy, Er, Eu, Gd, Ho, Lu, Tb, Tm, Yb, and Y), LREEs (light rare earth elements—Ce, La, Nd, Pr, and Sm), Li, Mg, Mn, Nb, P, Sb, Sc, Sr, Ta, W, and V; SRMs: Bi, Co, Ga, Ge, HREE, LREE, Li, Mg, Mn, Cu, Ni, W, and V. Other elements, e.g., In, Re, Sn, Se, Au, and Ag, are of economic importance but are not considered to be at risk of supply [7].

The concentrations of various elements found in the mining wastes analyzed are several times greater than the abundance in the Earth's crust, as shown in Figure 5. The considerable volume of certain waste associated with the presence of valuable metals raises questions about their sustainable recovery before rehabilitation procedures, e.g., [33,34].

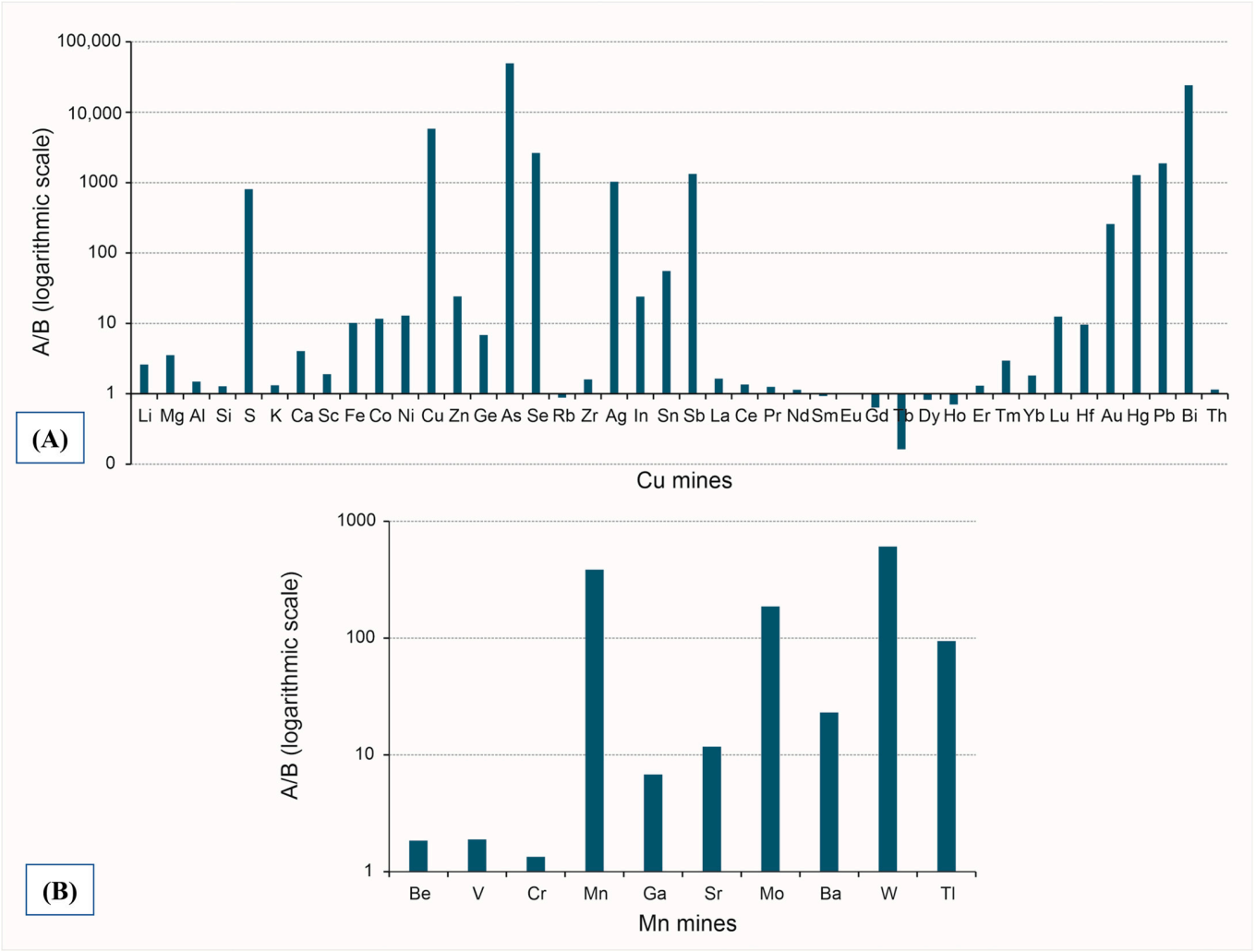

Figure 5. Ratio of the maximum content found in the wastes from Cu and Mn mines (**A**) and the abundance of chemical elements in the Earth's crust (**B**). Elements are ordered by atomic number (adapted from [35]).

With regards to the Cu mines, sample 1 from Porteirinhos is rich in Co, Cu, Mn, and Ni as critical and/or strategic raw materials, while sample 1 ore is concentrated in As, Co, Cu, Li, Mn, Ni, and Sb. This ore also has a high content of Ag, In, and S plus Si and sample 1 has a high content of Al and K plus Si. To link these elements to a mineralogical or carrier phase, XRD analysis was performed (Table 2). Some examples of the XRD spectra referred to in the following tables (Tables 2–4) can be seen in Figure 6. Due to the sample's mineralogical complexity, only a semi-quantitative approach was used to investigate the content of each phase. Phase identification was achieved using the analytical software, bearing in mind the elements previously identified by pXRF (Table S2). The main ore phases are quartz (SiO_2), chalcopyrite ($CuFeS_2$), and dolomite [$CaMg(CO_3)_2$]. A rough calculation gives about 18% chalcopyrite in the ore, considering all the copper at this phase. The same minerals are present in sample 1, but chalcopyrite is in vestigial, which led us to suppose that this waste material was discharged after ore processing; pseudomalachite, $Cu_5(PO_4)_2(OH)_4$, a

secondary mineral with low solubility found in oxidized zones of copper deposits [36], is also present.

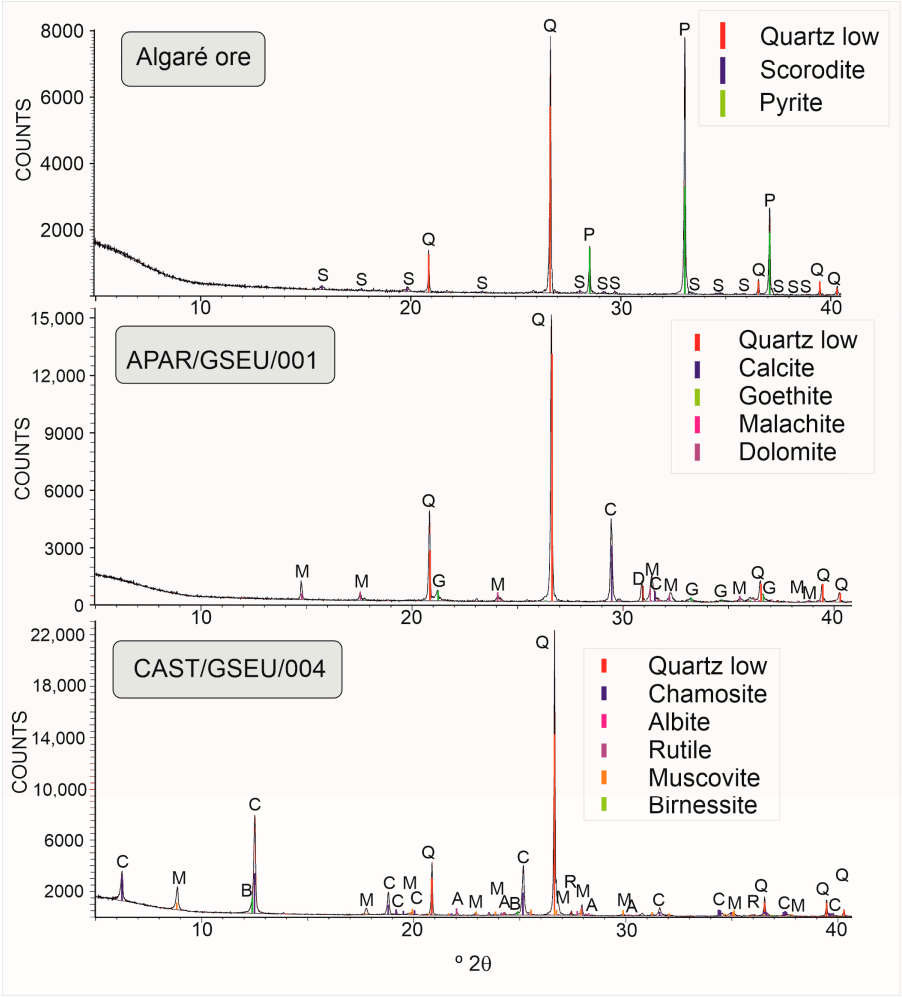

Figure 6. Illustrative examples of XRD spectra, as mentioned in Tables 2–4 (the name of the mineral phases in each spectrum is simplified using the first letter of the identified phase).

The same methodology was used for sample 1 ore from Cova dos Mouros (Table 2), rich in Se, Si, Sn, and W (the latter being both CRM and SRM), where quartz is the main gangue phase present. Tridymite is a high-temperature, low-pressure polymorph of silica. Two Mn phases were also identified, although in vestigial contents: Braunite, $Mn^{2+}Mn^{3+}{}_6(SiO_4)O_8$ and Manganite, $Mn^{3+}O(OH)$.

Samples 1 and 3 from Barrigão present the same mineralogical phases but in markedly different concentrations (Table 2). Copper phases—chalcopyrite, $CuFeS_2$, and tennantite—(Fe), $Cu_6(Cu_4Fe^{2+}{}_2)As_4S_{12}S$, are very well represented in the last sample, which is rich in Ag, Al, As, Bi, Cu, Ga, Ge, Li, S, Si, Sn, Zn, and REE (La, Ce, Nd, Sm, and Gd), making it the richest sample in Bi content of all wastes analyzed. From these elements, As, Bi, Cu, Ga, Ge, Li, and REE are considered critical or strategic. Sample 1 is only rich in Sb (CRM) and Si. A slag sample (BARR/GSEU/002) showed a high content of Al, K, Mn (CRM and SRM), Rb, Si, and Sr (CRM). It should be noted that the direct use of tennantite–tetrahedrite from the Barrigão mine dump has been studied for its application in thermoelectric (TE) material processing [37].

The XRD results of Algaré samples (Table 2) show the presence of scorodite, $Fe^{3+}AsO_4{\cdot}2H_2O$ (sample 1 and Algaré ore). This secondary mineral is a member of the

variscite group and results from the oxidation of arsenopyrite or other mineral species containing arsenic and is a very stable phase [38]. Quartz and pyrite (FeS_2) are also present. High concentrations of Ag, As (CRM), Au, Co (both a CRM and SRM), Fe, and In plus S were detected in sample 1 and As, Co, and Fe plus S in Algaré ore. Samples 2 and 3 are also mineralogically similar (mainly quartz and chamosite—$(Fe^{2+})_5Al(Si,Al)_4O_{10}(OH,O)_8$). Sample 2 also presents malachite, $Cu_2(CO_3)(OH)_2$ in a vestigial content (secondary mineral). Al, As, Co, Cu, Fe, Mn (CRM and SRM), Pb, Si, and Zn are concentrated in sample 2. Sample 3 has high contents of Al, As, Fe, and Si. Sample 4 is mainly constituted by quartz, hematite—Fe_2O_3, and kaolinite—$Al_2(Si_2O_5)(OH)_4$, having Al, Fe, Nb, Si, Sn, Y, and Zr in good concentrations. Sample 4 ore was collected nearby and was considered ore, presenting similar phases (quartz, hematite, and goethite—α-$Fe^{3+}O(OH)$). The chemical elements with high values are Fe, Ga, Hf, In, Nb, Sc, Si, Th, Zr, and REE (La, Ce, Nd, Gd, Tb, Ho, Er, Tm, Yb, Lu, and Y), with Ga, Hf, Nb, Sc, and REE considered critical and/or strategic raw materials.

Table 2. Mineralogical phases from Porteirinhos (PORT), Cova dos Mouros (CMOUR), Barrigão (BARR), and Algaré (ALG) samples identified by XRD (in alphabetical order for better visualization; symbols from IMA-CNMNC [39]). The main phases in each sample were roughly estimated as more (+++) or less (+) represented by the intensity of the principal lines. "+" signs indicate relative abundance of mineral. Legend: Ab—Albite, $Na(AlSi_3O_8)$; Alu—Alunite, $KAl_3(SO_4)_2(OH)_6$; Ank—Ankerite, $Ca(Fe^{2+},Mg)(CO_3)_2$; Ath—Anthophyllite, $\square\{Mg_2\}\{Mg_5\}(Si_8O_{22})(OH)_2$; Bir—Birnessite, $(Na,Ca)_{0.5}(Mn^{4+},Mn^{3+})_2O_4{\cdot}1.5H_2O$; Bnt—Braunite, $Mn^{2+}Mn^{3+}{}_6(SiO_4)O_8$; Btl—Butlerite, $Fe^{3+}(SO_4)(OH){\cdot}2H_2O$; Ccp—Chalcopyrite, $CuFeS_2$; Chm—Chamosite, $(Fe^{2+})_5Al(Si,Al)_4O_{10}(OH,O)_8$; Cld—Chloritoid, $(Fe^{2+},Mg,Mn^{2+})Al_2(SiO_4)O(OH)_2$; Cst—Cassiterite, SnO_2; Dol—Dolomite, $CaMg(CO_3)_2$; En—Enstatite, $Mg_2Si_2O_6$; Fau-Ca—Faujasite-Ca, $(Ca,Na_2,Mg)_{3.5}[Al_7Si_{17}O_{48}]{\cdot}32H_2O$; Gp—Gypsum, $CaSO_4{\cdot}2H_2O$; Gth—Goethite, α-$Fe^{3+}O(OH)$; Hem—Hematite, Fe_2O_3; Ilm—Ilmenite, $Fe^{2+}TiO_3$; Kln—Kaolinite, $Al_2(Si_2O_5)(OH)_4$; Mlc—Malachite, $Cu_2(CO_3)(OH)_2$; Mnn—Manganite, $Mn^{3+}O(OH)$; Ms/Bt—Muscovite/Biotite, $Al_2(AlSi_3O_{10})(OH)_2$/$K(Mg,Fe)_3AlSi_3O_{10}(OH)_2$; Mul—Mullite, $Al_{4+2x}Si_{2-2x}O_{10-x}$ (x~0.4); Ncr—Nacrite, $Al_2(Si_2O_5)(OH)_4$; Phl—Phlogopite, $KMg_3(AlSi_3O_{10})(OH)_2$; Pmlc—Pseudomalachite, $Cu_5(PO_4)_2(OH)_4$; Prl—Pyrophyllite, $Al_2Si_4O_{10}(OH)_2$; Py—Pyrite, FeS_2; Qz—Quartz, SiO_2; Rt—Rutile, TiO_2; Scd—Scorodite, $Fe^{3+}AsO_4{\cdot}2H_2O$; Tmgh—Titanomaghemite, $(Ti^{4+}{}_{0.5}\square_{0.5})Fe^{3+}{}_2O_4$; Tnt-Fe—Tennantite-(Fe), $Cu_6(Cu_4Fe^{2+}{}_2)As_4S_{12}S$; Trd—Tridymite, SiO_2; Var—Variscite, $AlPO_4{\cdot}2H_2O$; Zrn—Zircon, $Zr(SiO_4)$. Vtg: vestigial content; ?: dubious identification.

Sample Reference	Phase Identification	+++	++	+
PORT/GSEU/001	Ab + Bir + Ccp (vtg) + Chm + Dol + Ms/Bt + Pmlc (vtg) + Qz + Rt (vtg)	Quartz	Muscovite/Biotite, Chamosite, Albite	Birnessite, Dolomite
PORT/GSEU/001 Ore	Ank (vtg) + Bir (vtg) + Ccp + Chm (vtg) + Dol + En? (vtg) + Ms/Bt (vtg) + Qz + Var (vtg)	Quartz		Chalcopyrite, Dolomite
CMOUR/GSEU/001 Ore	Bnt (vtg) + Cst + Hem + Mnn (vtg) + Qz + Trd + Zrn (vtg)	Quartz		Cassiterite, Hematite, Tridymite
BARR/GSEU/001	Ccp (vtg) + Chm + Dol + Gp (vtg) + Kln (vtg) + Ms/Bt + Qz + Tnt-Fe (vtg)	Quartz		Dolomite, Chamosite, Musc./Biotite
BARR/GSEU/002	Ab + Mul + Qz +Tmgh (vtg)	Quartz	Mullite	Albite
BARR/GSEU/003	Ccp + Chm + Dol + Kln + Ms/Bt + Ncr + Qz + Tnt-Fe	Quartz	Tennantite-(Fe), Chalcopyrite, Kaolinite	Chamosite, Musc./Biotite, Dolomite

Table 2. *Cont.*

Sample Reference	Phase Identification	+++	++	+
ALG/GSEU/001	Alu (vtg) + Ath (vtg) + Btl (vtg) + Phl (vtg) + Prl (vtg) + Py + Qz + Scd	Quartz	Pyrite	Scorodite
ALG/GSEU/002	Chm + Cld (vtg) + Fau-Ca? (vtg) + Gth (vtg) + Hem (vtg) + Kln (vtg) + Mlc (vtg) + Ms/Bt + Qz	Quartz	Chamosite	Musc./Biotite
ALG/GSEU/003	Chm + Fau-Ca? (vtg) + Gth (vtg) + Kln (vtg) + Ms/Bt (vtg) + Qz	Quartz	Chamosite	
ALG/GSEU/004	Cld (vtg) + Gth (vtg) + Hem + Ilm (vtg) + Kln + Ms/Bt (vtg) + Qz	Quartz		Hematite, Kaolinite
ALG/GSEU/004 Ore	Gth + Hem + Kln (vtg) + Ms/Bt (vtg) + Qz	Quartz	Hematite	Goethite
Algaré Ore	Py + Qz + Scd	Quartz, Pyrite		Scorodite

Table 3. Semi-quantitative approach to the mineralogical content of Aparis (APAR) and Brancanes (BRAN) samples. The main phases in each sample were roughly estimated as more (+++) or less (+) represented by the intensity of the principal lines. "+" signs indicate relative abundance of mineral. Legend: Ab—Albite, $Na(AlSi_3O_8)$; An—Anorthite, $Ca(Al_2Si_2O_8)$; Ank—Ankerite, $Ca(Fe^{2+},Mg)(CO_3)_2$; Bct—Brochantite, $Cu_4(SO_4)(OH)_6$; Bir—Birnessite, $(Na,Ca)_{0.5}(Mn^{4+},Mn^{3+})_2O_4{\cdot}1.5H_2O$; Cal—Calcite, $CaCO_3$; Ccp—Chalcopyrite, $CuFeS_2$; Cer—Cerussite, $PbCO_3$; Chm—Chamosite, $(Fe^{2+})_5Al(Si,Al)_4O_{10}(OH,O)_8$; Cpr—Cuprite, Cu_2O; Dol—Dolomite, $CaMg(CO_3)_2$; Fa—Fayalite, $Fe^{2+}{}_2SiO_4$; Gp—Gypsum, $CaSO_4{\cdot}2H_2O$; Gth—Goethite, α-$Fe^{3+}O(OH)$; Hem—Hematite, Fe_2O_3; Kln—Kaolinite, $Al_2(Si_2O_5)(OH)_4$; Mag—Magnetite, $Fe^{2+}Fe^{3+}{}_2O_4$; Mlc—Malachite, $Cu_2(CO_3)(OH)_2$; Ms/Bt—Muscovite/Biotite, $Al_2(AlSi_3O_{10})(OH)_2/K(Mg,Fe)_3AlSi_3O_{10}(OH)_2$; Mul—Mullite, $Al_{4+2x}Si_{2-2x}O_{10-x}$ (x~0.4); Qz—Quartz, SiO_2; Spl—Spinel, $MgAl_2O_4$; Tns—Ternesite, $Ca_5(SiO_4)_2(SO_4)$; Tnt-Fe—Tennantite-(Fe), $Cu_6(Cu_4Fe^{2+}{}_2)As_4S_{12}S$; Wwf—Wroewolfeite, $Cu_4(SO_4)(OH)_6{\cdot}2H_2O$. Vtg: vestigial content; ?: dubious identification.

Sample Reference	Phase Identification	+++	++	+
APAR/GSEU/001	Cal + Dol + Gth + Mlc + Qz	Quartz	Calcite	Goethite, Malachite, Dolomite
APAR/GSEU/002	Bir (vtg) + Ccp + Chm (vtg) + Dol + Ms/Bt (vtg) + Qz	Quartz, Dolomite		Chalcopyrite
APAR/GSEU/003	Bct (vtg) + Ccp + Chm (vtg) + Dol + Mlc (vtg) + Ms/Bt (vtg) + Qz	Quartz	Dolomite	Chalcopyrite
APAR/GSEU/004	Ank (vtg) + Cal (vtg) + Cer (vtg) + Chm + Cpr (vtg) + Dol + Ms/Bt + Qz	Quartz	Dolomite	Chamosite, Muscovite/Biotite
APAR/GSEU/005	Chm + Dol + Ms/Bt + Qz	Quartz	Dolomite	Chamosite, Muscovite/Biotite
APAR/GSEU/006	Chm + Dol + Ms/Bt + Qz	Quartz	Dolomite	Chamosite, Muscovite/Biotite

Table 3. *Cont.*

Sample Reference	Phase Identification	+++	++	+
APAR/GSEU/007	Chm + Dol + Ms/Bt + Qz	Quartz		Dolomite, Chamosite, Muscovite/Biotite
BRAN/GSEU/001	Ab + An + Fa + Mag + Mul + Qz + Spl(1) + Spl(2) + Tns	Spinel(1), Anorthite, Albite	Magnetite, Spinel(2), Fayalite	Quartz,Mullite, Ternesite
BRAN/GSEU/002	Ank + Dol + Gp + Kln + Mlc + Ms/Bt + Qz	Quartz	Dolomite, Gypsum, Ankerite	Muscovite/Biotite, Malachite, Kaolinite
BRAN/GSEU/003	Ab (vtg) + Hem (vtg) + Mag + Mul + Qz	Quartz		Mullite, Magnetite
Brancanes Ore	Ccp + Dol + Gp (vtg) + Qz + Tnt? (vtg) + Wwf (vtg)	Dolomite		Chalcopyrite, Quartz

Table 4. Semi-quantitative approach to the mineralogical content of Ferragudo (FERR), Ferrarias e Castelo (CAST), Cêrro do Serpe (SERP), and Balança (BALA) samples. The main phases in each sample were roughly estimated as more (+++) or less (+) represented by the intensity of the principal lines. "+" signs indicate relative abundance of mineral. Legend: Ab—Albite, $Na(AlSi_3O_8)$; Alm—Almandine, $Fe^{2+}{}_3Al_2(SiO_4)_3$; Ank—Ankerite, $Ca(Fe^{2+},Mg)(CO_3)_2$; Bir—Birnessite, $(Na,Ca)_{0.5}(Mn^{4+},Mn^{3+})_2O_4{\cdot}1.5H_2O$; Bnt—Braunite, $Mn^{2+}Mn^{3+}{}_6(SiO_4)O_8$; Bob—Bobierrite, $Mg_3(PO_4)_2{\cdot}8H_2O$; Cbz-Ca—Chabazite-Ca, $(Ca,K_2,Na_2)_2[Al_2Si_4O_{12}]_2{\cdot}12H_2O$; Chm—Chamosite, $(Fe^{2+})_5Al(Si,Al)_4O_{10}(OH,O)_8$; Clb-Fe—Columbite-(Fe), $Fe^{2+}Nb_2O_6$; Cpr-Cuprite, Cu_2O; Dpt—Dioptase, $CuSiO_3{\cdot}H_2O$; Fau-Na—Faujasite-Na, $(Na_2,Ca,Mg)_{3.5}[Al_7Si_{17}O_{48}]{\cdot}32H_2O$; Gh—Gehlenite, $Ca_2Al[AlSiO_7]$; Gnp—Ganophyllite, $(K,Na,Ca)_2Mn_8(Si,Al)_{12}(O,OH)_{32}{\cdot}8H_2O$; Gp—Gypsum, $CaSO_4{\cdot}2H_2O$; Mnn—Manganite, $Mn^{3+}O(OH)$; Mog—Mogánite, SiO_2; Hem—Hematite, Fe_2O_3; Hsm—Hausmannite, $Mn^{2+}Mn^{3+}{}_2O_4$; Mnt—Montmorillonite, $(Na,Ca)_{0.33}(Al,Mg)_2(Si_4O_{10})(OH)_2{\cdot}nH_2O$; Ms/Bt—Muscovite/Biotite, $Al_2(AlSi_3O_{10})(OH)_2/K(Mg,Fe)_3AlSi_3O_{10}(OH)_2$; Ncr—Nacrite, $Al_2(Si_2O_5)(OH)_4$; Phl—Phlogopite, $KMg_3(AlSi_3O_{10})(OH)_2$; Pyc—Pyrochroite, $Mn(OH)_2$; Pyl—Pyrolusite, $Mn^{4+}O_2$; Qz—Quartz, SiO_2; Rds—Rhodochrosite, $MnCO_3$; Rt—Rutile, TiO_2; Sd—Siderite, $FeCO_3$; Sid—Siderophyllite, $KFe^{2+}{}_2Al(Al_2Si_2O_{10})(OH)_2$; Sps—Spessartine, $Mn^{2+}{}_3Al_2(SiO_4)_3$, Whm—Whitmoreite, $Fe^{2+}Fe^{3+}{}_2(PO_4)_2(OH)_2{\cdot}4H_2O$. Vtg: vestigial content; ?: dubious identification.

Sample Reference	Phase Identification	+++	++	+
FERR/GSEU/001	Ab + Alm calcian + Cbz-Ca (vtg) + Chm + Dpt + Gnp (vtg) + Gp (vtg) + Hsm + Mnt (vtg) + Phl (vtg) + Qz + Rds	Rhodochrosite, Quartz	Albite	Dioptase, Hausmannite, Almandine calcian, Chamosite
FERR/GSEU/002	Ab (vtg) + Alm calcian + Bir (vtg) + Fau-Na (vtg) + Ms/Bt (vtg) + Pyl + Qz + Sps	Quartz		Pyrolusite, Almandine calcian, Spessartine
FERR/GSEU/003	Ab (vtg) + Bir (vtg) + Chm (vtg) + Mnt (vtg) + Ms/Bt + Qz + Rt (vtg)	Quartz		Muscovite/Biotite
FERR/GSEU/004	Ab (vtg) + Alm calcian + Bir + Fau-Na + Mnt (vtg) + Ms/Bt (vtg) + Qz + Sps	Quartz	Faujasite-Na, Almandine calcian, Spessartine	Birnessite

Table 4. *Cont.*

Sample Reference	Phase Identification	+++	++	+
CAST/GSEU/001	Ab (vtg) + Bir (vtg) + Chm (vtg) + Mnn + Qz + Rds + Sid (vtg)	Rhodochrosite		Quartz, Manganite
CAST/GSEU/002	Ab (vtg) + Bir (vtg) + Chm + Clb-Fe? (vtg) + Cpr (vtg) + Hem (vtg) + Ms/Bt (vtg) + Py (vtg) + Pyc (vtg) + Qz + Rds + Rt (vtg) + Sd	Quartz	Chamosite	Rhodochrosite, Siderite
CAST/GSEU/003	Ab (vtg) + Ank (vtg) + Bir (vtg) + Chm + Gh? (vtg) + Hem (vtg) + Qz + Rds + Sd + Whm? (vtg)	Chamosite	Quartz	Rhodochrosite, Siderite
CAST/GSEU/004	Ab (vtg) + Bir (vtg) + Chm + Ms/Bt + Qz + Rt (vtg)	Quartz	Chamosite	Muscovite/Biotite
SERP/GSEU/001 Ore	Ab + Bob? (vtg) + Mog (vtg) + Pyl + Qz	Quartz		Albite, Pyrolusite
BALA/GSEU/001	Ab + Bnt + Hem + Ncr? (vtg) + Pyl + Qz (vtg) + Rds	Rhodochrosite, Braunite	Pyrolusite	Hematite, Albite

Quartz and dolomite [$CaMg(CO_3)_2$] are present in all samples from Aparis (Table 3). Several Cu phases were also identified, and among those were malachite (APAR/GSEU/001) and chalcopyrite (samples 2 and 3). Similar critical and strategic raw materials were found (As, Cu, and Mn). Samples 5–7 are mineralogically identical and do not have significant CRMs or SRMs. Although sample 4 is also identical, the presence of Li, Mg, and REE (Ce, Nd, and Sm) should be highlighted.

Two slag samples from Brancanes (1 and 3) contain minerals such as fayalite, mullite, and several spinels (Table 3). High contents of Al, Ba, Co, Fe, Mn, Ni, and Si plus Sr were found in sample 1, while Al, As, Ca, Co, Cs, Cu, K, Mg, Mn, Ni, Rb, Sb, Si, Th, and REE (La, Ce, Pr, Nd, Sm, Eu, and Gd) were found in sample 2: CRMs (As, Co, Mg, Mn, Sb, Sr, and REE), SRMs (Co, Cu, Mg, Mn, Ni, and REE). Sample 2 is rich in Al, Ba, Fe, and Mn plus Sr and Brancanes ore is rich in As, Ca, Cu, In, Mg, Mn, Ni, S, and Sb plus REE (Gd, Dy). This last sample has the highest Ni content of all wastes studied (750 ppm).

The mineralogy of the Lousal samples studied previously [33] mainly showed the presence of pyrite, quartz, mica (muscovite or biotite), feldspar (albite), chlorite (chamosite), and numerous neogenic sulphates with variable degrees of hydration, of which gypsum ($CaSO_4{\cdot}2H_2O$), rhomboclase [$(H_5O_2)Fe^{3+}(SO_4)_2{\cdot}2H_2O$], ferricopiapite [$Fe^{3+}{}_{0.67}Fe^{3+}{}_4(SO_4)_6(OH)_2{\cdot}20H_2O$], coquimbite [$AlFe_3(SO_4)_6(H_2O)_{12}{\cdot}6H_2O$], and jarosite [$KFe_3{}^{+3}(SO_4)_2(OH)_6$] stood out. New chemical analyses of the two samples were performed in ACTLABS for comparison purposes (Table S2). For instance, interesting values of Au (sample 1) and Ag (samples 1 and 14) were obtained. A higher content of Sb and Pb is present in samples 1, 9, 10, and 14, while As is concentrated in samples 10, 11, 12, and 14. Sample 4 is rich in several CRMs and SRMs, Hf, Ga, Nb, Sc, V, and REE (La, Ce, Pr, Nd, Sm, Eu, Gd, Dy, Tb, and Er plus Yb), sample 1 is rich in Co and Ce, samples 3 and 8 are rich in Mn, and sample 14 is rich in Sr.

In the Mn mines, several phases with Mn were identified in the Ferragudo samples (Table 4), namely hausmannite ($Mn^{2+}Mn^{3+}{}_2O_4$), pyrolusite ($Mn^{4+}O_2$), birnessite

[$(Na,Ca)_{0.5}(Mn^{4+},Mn^{3+})_2O_4 \cdot 1.5H_2O$], ganophyllite [$(K,Na,Ca)_2Mn_8(Si,Al)_{12}(O,OH)_{32} \cdot 8H_2O$], rhodochrosite ($MnCO_3$), and spessartine [$Mn^{2+}{}_3Al_2(SiO_4)_3$] with Mn in various oxidation states. This critical and raw material is concentrated in all samples (Table S2). Sample 1 is rich in Ba, Be, Ce, Co, Cs, Mo, V, and W, while sample 2 has a high content of Ba, Be, Ce, Co, Cs, Mo, Nb, Rb, Si, Sr, Th, U, V, W, Zn, and REE (Y, La, Nd, Eu, Gd, Dy, Tb, Er, and Yb). These two samples have the highest Mo content of all wastes analyzed. Sample 3 is less rich with good values only for Al, K, and Rb plus Si, while sample 4 has high levels of Co, V, and W. The presence of spessartine is an indicator of temperature conditions above those regularly quoted for massive primary Mn(-Fe) oxide ores in the IPB (>350 °C) [40].

The mineralogy of the Ferrarias and Castelo samples (Table 4) revealed two new Mn-phases: manganite [$Mn^{3+}O(OH)$] and pyrochroite [$Mn(OH)_2$]. Mn is concentrated in all samples. Sample 1 is rich in Ba, Fe, and Sr, while sample 2 has high concentrations of Ba, Co, Cr, Fe, Nb, V, and REE (Nd). Sample 3 displays high contents of Ba and Cr plus Sr; however, sample 4 is rich in Cr, Nb, and Si.

The sample ore from Cêrro do Serpe displays quartz, albite, and pyrolusite as the main phases (Table 4) and high contents of Ba, Be, Co, Ga, Mn, Si, and Sr plus W. It also shows remarkable concentrations of Ba (1.5%) and Ga (129 ppm), with the latter being both a CRM and SRM.

Several Mn phases are present in the Balança sample (Table 4): rhodochrosite, braunite [$Mn^{2+}Mn^{3+}{}_6(SiO_4)O_8$], and pyrolusite. The chemical elements with high contents are Ba, Be, Mn, Sr, and Tl (with Mn content reaching about 48%). Although not considered critical or strategic, Tl is very well represented in this waste sample (94 ppm).

Table 5 depicts a summary of where to search for CRM and/or SRM on the samples analyzed, according to the chemical contents obtained. The waste volume was not considered in this first approach. Heavy rare earth elements (HREEs) include Dy, Er, Eu, Gd, Ho, Lu, Tb, Tm, Yb, and Y, while light rare earth elements represent Ce, La, Nd, Pr, and Sm [7].

Table 5. Distribution of relevant CRM and/or SRM contents in the samples analyzed according to the 2023 list published by the EU Commission [7].

Sample Reference	Sb	As	Bi	Co	Cu	Ga	Ge	Hf	HREE	Li	LREE	Mg	Mn	Ni	Nb	Sc	Sr	W	V
PORT/GSEU/001					X														
PORT/GSEU/001 Ore	X	X		X	X					X			X	X					
CMOUR/GSEU/001 Ore																		X	
BARR/GSEU/001	X	X			X							X							
BARR/GSEU/002																	X		
BARR/GSEU/003		X	X		X	X	X		X	X	X								
ALG/GSEU/001		X		X															
ALG/GSEU/002		X			X														
ALG/GSEU/003		X																	
ALG/GSEU/004															X				
ALG/GSEU/004 Ore		X				X		X	X		X					X			
Algaré Ore																			
APAR/GSEU/001					X														
APAR/GSEU/002					X														
APAR/GSEU/003					X														
APAR/GSEU/004										X	X	X							
APAR/GSEU/005																			
APAR/GSEU/007																			
BRAN/GSEU/001																	X		

Table 5. *Cont.*

Sample Reference	Sb	As	Bi	Co	Cu	Ga	Ge	Hf	HREE	Li	LREE	Mg	Mn	Ni	Nb	Sc	Sr	W	V
BRAN/GSEU/002	X	X		X	X							X	X	X					
BRAN/GSEU/003									X		X						X		
Brancanes Ore	X	X			X							X	X	X					
LOUS/GSEU/001	X			X					X										
LOUS/GSEU/002											X								
LOUS/GSEU/003																			
LOUS/GSEU/004						X		X	X		X				X	X			X
LOUS/GSEU/006																			
LOUS/GSEU/007																			
LOUS/GSEU/008																			
LOUS/GSEU/009																			
LOUS/GSEU/010																			
LOUS/GSEU/011																			
LOUS/GSEU/012																			
LOUS/GSEU/013																			
LOUS/GSEU/014																	X		
FERR/GSEU/001				X							X		X					X	X
FERR/GSEU/002				X					X		X		X		X		X	X	X
FERR/GSEU/003													X						
FERR/GSEU/004													X						
CAST/GSEU/001													X				X		
CAST/GSEU/002				X							X		X		X				X
CAST/GSEU/003													X				X		
CAST/GSEU/004												X	X						
SERP/GSEU/001 Ore				X		X							X				X	X	
BALA/GSEU/001PORT1													X				X		

4. Conclusions

The performance of the XRF portable equipment in mineralogically complex mine waste samples was evaluated. No significant differences in the element concentrations were observed between performing one or an average of three measures collected in different points/areas of the same sample, which suggests good precision of the equipment. The accuracy of the pXRF equipment, tested through a comparison with element concentrations obtained for selected samples in a certified international laboratory (ACTLABS) and with XRF laboratory equipment (WDS), showed good correlations for Al, As, Ba, Ca, Cu, Fe, Ga, K, Mg, Mn, Mo, Ni, Pb, Rb, S, Sb, Se, Si, Sr, Ti, Zn, and W. Therefore, the use of pXRF equipment has proven to be useful for a quick and inexpensive overview (both in the field and in the laboratory) of the many elements that a waste sample can contain.

The high concentrations of Fe (47.4%), Cu (27.5%), As (8.4%), Pb (3%), and Sn (139 ppm) found in wastes from old Cu mines are consistent with the various minerals identified, namely, chalcopyrite [$CuFeS_2$], pyrite [FeS_2], tennantite-(Fe) [$Cu_6(Cu_4Fe^{2+}{}_2)As_4S_{12}S$], cuprite [$Cu_2O$], malachite [$Cu_2(CO_3)(OH)_2$], pseudomalachite [$Cu_5(PO_4)_2(OH)_4$], brochantite [$Cu_4(SO_4)(OH)_6$], wroewolfeite [$Cu_4(SO_4)(OH)_6{\cdot}2H_2O$], jarosite [$KFe_3{}^{+3}(SO_4)_2(OH)_6$], butlerite [$Fe^{3+}(SO_4)(OH){\cdot}2H_2O$], rhomboclase [$(H_5O_2)Fe^{3+}(SO_4)_2{\cdot}2H_2O$], ferricopiapite [$Fe^{3+}{}_{0.67}Fe^{3+}{}_4(SO_4)_6(OH)_2{\cdot}20H_2O$], coquimbite [$AlFe_3(SO_4)_6(H_2O)_{12}{\cdot}6H_2O$], ankerite [$Ca(Fe^{2+},Mg)(CO_3)_2$], fayalite [$Fe^{2+}{}_2SiO_4$], chamosite [$(Fe^{2+})_5Al(Si,Al)_4O_{10}(OH,O)_8$], chloritoid [$(Fe^{2+},Mg,Mn^{2+})Al_2(SiO_4)O(OH)_2$], hematite [$Fe_2O_3$], magnetite [$Fe^{2+}Fe^{3+}{}_2O_4$], goethite [$\alpha$-$Fe^{3+}O(OH)$], ilmenite [$Fe^{2+}TiO_3$], titanomaghemite [$(Ti^{4+}{}_{0.5}\square_{0.5})Fe^{3+}{}_2O_4$], scorodite [$Fe^{3+}AsO_4{\cdot}2H_2O$], cerussite [$PbCO_3$], and cassiterite [$SnO_2$]. Minor and vestigial contents of Mg (6.6%), Ni (750 ppm), Sb (665 ppm), Zr (271 ppm), Bi (217 ppm), Co (209 ppm), Rb (132 ppm), Se (132 ppm), Li (83 ppm), Ag (72 ppm), Sc (19 ppm), Th (14.9 ppm), Hf (9.6 ppm), Ge (9.6 ppm), In (6 ppm), Au (1110 ppb), and REE (La—47.6 ppm,

Ce—94.7, Pr—11.3, Nd—42.1, Sm—7.4, Eu—1.28, Gd—5.1, Dy—4.1, Tb—0.7, Ho—1.2, Er—4.3, Tm—0.8, Yb—6, and Lu—1 ppm) were also found.

Conversely, the Mn minerals identified in mine waste dumps from the studied Mn mines were hausmannite [$Mn^{2+}Mn^{3+}{}_2O_4$], pyrolusite [$Mn^{4+}O_2$], birnessite [$(Na,Ca)_{0.5}(Mn^{4+},Mn^{3+})_2O_4 \cdot 1.5H_2O$], ganophyllite [$(K,Na,Ca)_2Mn_8(Si,Al)_{12}(O,OH)_{32} \cdot 8H_2O$], manganite [$Mn^{3+}O(OH)$], pyrochroite [$Mn(OH)_2$], rhodochrosite [$MnCO_3$], spessartine [$Mn^{2+}{}_3Al_2(SiO_4)_3$], and braunite [$Mn^{2+}Mn^{3+}{}_6(SiO_4)O_8$]. The Mn concentration reached 38.6% in waste materials, where Ba (1.5%), Sr (0.4%), W (790 ppm), V (170 ppm), Mo (205 ppm), Ga (129 ppm), Cr (111 ppm), Tl (94.4 ppm), and Be (7 ppm) were also observed.

Studying mine waste is a crucial step toward sustainable resource management and environmental stewardship, ensuring economic and ecological resilience with obvious environmental and economic gains, ensuring global competitiveness, and fostering the circular economy. Furthermore, the study of mine waste is critical in addressing resource supply challenges and mitigating environmental impacts (e.g., acid mine drainage, AMD).

Although we are lacking total volume calculation for these mine wastes, the study reveals the importance of knowing the chemical and mineralogical potential of mining wastes of abandoned mines in order to potentially increase CRM and SRM sources, use them in the waste-to-value recycling process, and reduce potential environmental impacts.

Supplementary Materials: The following supporting information can be downloaded at: https://www.mdpi.com/article/10.3390/min15010058/s1, Table S1: Chemical characterization of waste materials: comparison of results obtained through ACTLABS, pXRF, and XRF laboratory equipment; Table S2: Chemical analyses performed on wastes from copper and manganese abandoned mines.

Author Contributions: T.P.S.; methodology, D.P.S.d.O., T.P.S. and I.M.; software, T.P.S.; validation, D.P.S.d.O., T.P.S. and I.M.; investigation, D.P.S.d.O., T.P.S., I.M. and J.A.E.F.; data curation, T.P.S. and J.A.E.F.; writing—original draft preparation, D.P.S.d.O., T.P.S. and I.M.; writing—review and editing, D.P.S.d.O., T.P.S., I.M. and J.A.E.F.; visualization, D.P.S.d.O., T.P.S. and I.M.; supervision, D.P.S.d.O., T.P.S., and I.M. All authors have read and agreed to the published version of the manuscript.

Funding: This research was partly funded by the Geological Service for Europe project (GSEU), Grant Agreement number 101075609—GSEU—HORIZON-CL5-2021-D3-02, and through the funds of LNEG.

Data Availability Statement: All new research data acquired and used in this study are published herein.

Acknowledgments: The authors would like to thank the revision and comments from four anonymous reviewers who have improved the manuscript.

Conflicts of Interest: The authors declare no conflicts of interest.

References

1. Council of the European Communities. Resolution of the Council of the European Communities and of the Representatives of the Governments of the Member States Meeting Within the Council of May 1977 on the continuation and implementation of a European Community policy and action programme on the environment. *Off. J. Eur. Commun.* **1977**, *139*, 1–46. Available online: https://eur-lex.europa.eu/legal-content/EN/TXT/?uri=CELEX:41977X0613 (accessed on 5 December 2024).
2. European Commission. The Raw Materials Initiative—Meeting Our Critical Needs for Growth and Jobs in Europe, Communication from the Commission to the European Parliament and the Council, COM (2008) 699 Final. Available online: https://eur-lex.europa.eu/legal-content/EN/ALL/?uri=CELEX:52008DC0699 (accessed on 21 October 2024).
3. European Commission. A Secure and Sustainable Supply of Critical Raw Materials in Support of the Twin Transition, Communication from the Commission to the European Parliament, the Council, the European Economic and Social Committee and the Committee of the Regions, COM (2023) 165 Final. Available online: https://eur-lex.europa.eu/legal-content/EN/TXT/?uri=COM:2023:165:FIN (accessed on 21 October 2024).

4. Rizos, V.; Righetti, E. Low-carbon technologies and Russian imports: How far can recycling reduce the EU's raw material dependency? *CEPS Policy Insight* **2022**, *2022–17*, 36180, Centre for European Policy Studies..
5. Righetti, E.; Rizos, V. The EU's Quest for Strategic Raw Materials: What Role for Mining and Recycling? *Intereconomics* **2023**, *58*, 69–73. Available online: https://www.intereconomics.eu/pdf-download/year/2023/number/2/article/the-eu-s-quest-for-strategic-raw-materials-what-role-for-mining-and-recycling.html (accessed on 4 December 2024). [CrossRef]
6. Hool, A.; Helbig, C.; Wierink, G. Challenges and opportunities of the European Critical Raw Materials Act. *Miner. Econ.* **2024**, *37*, 661–668. [CrossRef]
7. Grohol, M.; Veeh, C.; European Commission. Study on the Critical Raw Materials for the EU: Final Report, Publications Office of the European Union. 2023. Available online: https://data.europa.eu/doi/10.2873/725585 (accessed on 10 September 2024).
8. European Commission. Proposal for a Regulation of the European Parliament and of the Council Establishing a Framework for Ensuring a Secure and Sustainable Supply of Critical Raw Materials and Amending Regulations (EU) 168/2013, (EU) 2018/858, 2018/1724 and (EU) 2019/1020, COM/2023/160 Final. 2023. Available online: https://eur-lex.europa.eu/legal-content/EN/TXT/?uri=CELEX:52023PC0160 (accessed on 4 October 2024).
9. Carvalho, J.; Diamantino, C.; Rosa, C.; Carvalho, E. Potential recovery of mineral resources from mining tailings of abandoned mines in Portugal. In Proceedings of the 3rd International Symposium on Enhanced Landfill Mining, Lisbon, Portugal, 8–10 February 2016; Pereira, M.J., Carvalho, M.T., Neves, P.F., Eds.; Instituto Superior Técnico: Lisbon, Portugal, 2016; pp. 501–516, ISBN 978-989-98342-4-8.
10. Hu, X.; Yang, H.; Wu, F.; Fang, X.; Tan, K. Recovery of copper-dominated resources from copper mine drainage by chemical oxidation and sulfur biocycling: A pilot-scale study. *J. Clean. Prod.* **2022**, *378*, 134525. [CrossRef]
11. Sánchez-Andrea, I.; Stams, A.J.M.; Weijma, J.; Contreras, P.G.; Dijkman, H.; Rozendal, R.A.; Johnson, D.B. A case in support of implementing innovative bio-processes in the metal mining industry. *FEMS Microbiol. Lett.* **2016**, *363*, fnw106. [CrossRef] [PubMed]
12. Mohanty, S.; Ghosh, S.; Bal, B.; Das, A.P. A review of biotechnology processes applied for manganese recovery from wastes. *Rev. Environ. Sci. Biotechnol.* **2018**, *17*, 791–811. [CrossRef]
13. Euro Manganese Inc. Chvaletice Manganese Project. 2024. Available online: https://www.mn25.ca/chvaletice-manganese-project (accessed on 23 September 2024).
14. Neves, F.; Esperto, L.; Figueira, I.; Mascarenhas, J.; Salgueiro, R.; Silva, T.P.; Correia, J.B.; Carvalho, P.A.; de Oliveira, D. Mechanochemical synthesis of tetrahedrite materials using mixtures of synthetic and ore samples collected in the Portuguese zone of the Iberian Pyrite Belt. *Miner. Eng.* **2021**, *164*, 106833. [CrossRef]
15. de Oliveira, D.P.S.; Filipe, A.; Gonçalves, P.; Santos, S.; Albardeiro, L. Critical Raw Materials Deposits Map of Mainland Portugal: New Mineral Intelligence in Cartographic Form. *Cartog. J.* **2021**, *58*, 222–232. [CrossRef]
16. Tornos, F.; Inverno, C.M.C.; Casquet, C.; Mateus, A.; Ortiz, G.; Oliveira, O. The metallogenic evolution of the Ossa-Morena Zone. *J. Iber. Geol.* **2004**, *30*, 143–181.
17. Sáez, R.; González, F.; Donaire, T.; Toscano, M.; Yesares, L.; de Almodóvar, G.R.; Moreno, C. Updating Geological Information about the Metallogenesis of the Iberian Pyrite Belt. *Minerals* **2024**, *14*, 860. [CrossRef]
18. Díez-Montes, A.; Matos, J.X.; Dias, R.; Carmona, J.J.H.; Albardeiro, L.; Oliveira, J.T.; Morais, I.; Fernandes, P.; Inverno, C.; Machado, S.; et al. Geological Map of the South Portuguese Zone, Mapa Geológico de la Zona Surportuguesa/Carta Geológica da Zona Sul Portuguesa, Escala 1/400 000. Proj. Geo-FPI/Interreg POCTEP; Instituto Geológico y Minero de España/LNEG/Junta de Andalucía-SGIEM/CM Aljustrel. 2020. Available online: https://info.igme.es/geofpi/docs/mapas/GEOLOGICO_400K_ZSP_2020.pdf (accessed on 10 December 2024).
19. Piçarra, J.M. Estudo Estratigráfico do Sector de Estremoz—Barrancos, Zona de Ossa Morena, Portugal. Ph.D. Thesis, University of Évora, Évora, Portugal, 2000; Volume I and II, 268p.
20. Gaspar, O.C. O Jazigo de Cobre de Aparis. *Est. Not. Trab. SFM* **1968**, *18*, 253–290.
21. Matos, J.X.; Rosa, C. Diagnóstico Preliminar de Minas Abandonadas—Área Sul. In *Internal IGM Report*; IGM Eds.: Lisbon, Portugal, 2001; 276p.
22. Matos, J.X.; Martins, L.; Rosa, C. Parque Mineiro da Cova dos Mouros—IGM: Contribution for the sustainable development of the mining park. *IGME Pub. Mus. Geom.* **2003**, *2*, 487–494.
23. Reiser, F.K.M.; Rosa, D.R.N.; Pinto, Á.M.M.; Carvalho, J.R.S.; Matos, J.X.; Guimarães, F.M.G.; Alves, L.C.; de Oliveira, D.P.S. Mineralogy and geochemistry of tin- and germanium-bearing copper ore, Barrigão re-mobilized vein deposit, Iberian Pyrite Belt, Portugal. *Int. Geol. Rev.* **2011**, *53*, 1212–1238. [CrossRef]
24. Matos, J.X. Recursos geológicos—Minérios metálicos. In *Notícia Explicativa da Folha 46D Mértola*; Oliveira, J.T., Silva, J.B., Eds.; Dep. Geologia INETI: Lisbon, Portugal, 2007; pp. 28–34.
25. Sáez, R.; Pascual, E.; Toscano, M.; Almodóvar, G. The Iberian type of volcano-sedimentary massive sulphide deposits. *Mineral. Depos.* **1999**, *34*, 549–570. [CrossRef]

26. Matos, J.X.; Martins, L.P.; Oliveira, J.T.; Pereira, Z.; Batista, M.J.; Quental, L. Rota da pirite no sector português da Faixa Piritosa Ibérica, desafios para um desenvolvimento sustentado do turismo geológico e mineiro. In *Rutas Minerales en Iberoamérica*; Carrion, P., Ed.; Esc. Sup. Politécnica del Litoral: Guayaquil, Equador, 2008; pp. 136–155.
27. Oliveira, J.T.; Relvas, J.; Pereira, Z.; Matos, J.X.; Rosa, C.; Rosa, D.; Munhá, J.M.; Fernandes, P.; Jorge, R.; Pinto, A. Geologia da Zona Sul Portuguesa, com ênfase na estratigrafia e na vulcanologia física, geoquímica e mineralizações da Faixa Piritosa. In *Geologia de Portugal Vol. I—Geologia Pré-Mesozóica de Portugal*; Dias, R., Araújo, A., Terrinha, P., Kullberg, J., Eds.; Escolar Editora: Lisbon, Portugal, 2013; pp. 673–767.
28. Pinedo Vara, I. *Piritas de Huelva. Su Historia, Minería y Aprovechamiento*; Edit. Summa: Madrid, Spain, 1963; 1003p.
29. Fernandes, C. Jazigos de Mn do Alentejo. Breve estudo das minas de Mn do concelho de Castro Verde. In *Internal IGM Report*; IGM Eds.: Lisbon, Portugal, 1947.
30. Goinhas, F. *Minas de Manganês do Baixo Alentejo. Internal Report from DGGM*; DGGM Eds.: Lisbon, Portugal, 1986.
31. Silva, F. Géologie et génese des gisements de Manganese du Baixo Alentejo Portugal. *Est. Not. Trab. SFM* **1956**, *XI*, 28–66.
32. Lohmeier, S.; Gallhofer, D.; Lottermoser, B.G. Field-portable X-ray fluorescence analyzer for chemical characterization of carbonate-bearing base metal tailings: Case study from Namib Pb-Zn Mine, Namibia. *J. South. Afr. Inst. Min. Metall.* **2024**, *124*, 421–436. [CrossRef]
33. Figueiredo, M.O.; Silva, T.P.; Veiga, J.P.; de Oliveira, D.; Batista, M.J. Towards the recovery of by-product metals from mine wastes: An X-ray absorption spectroscopy study on the binding state of rhenium in debris from a centennial Iberian Pyrite Belt mine. *J. Miner. Mater. Charact. Eng.* **2014**, *2*, 135–143. [CrossRef]
34. de Oliveira, D.; Gonçalves, P.; Morais, I.; Silva, T.P.; Matos, J.X.; Albardeiro, L.; Filipe, A.; Batista, M.J.; Santos, S.; Fernandes, J. Unlocking the secondary critical raw material potential of historical mine sites, Lousal Mine, southern Portugal. *Minerals* **2024**, *14*, 127. [CrossRef]
35. Yaroshevsky, A.A. Abundances of Chemical Elements in the Earth's Crust. *Geochem. Int.* **2006**, *44*, 48–55. [CrossRef]
36. Abreu, M.M.; Matias, M.J.; Magalhães, M.C.F.; Basto, M.J. Impacts on water, soil and plants from the abandoned Miguel Vacas copper mine, Portugal. *J. Geochem. Explor.* **2008**, *96*, 161–170. [CrossRef]
37. De Oliveira, D.; Salgueiro, R.; Silva, T.P.; Reiser, F.; Guimarães, F.; Neves, F. The Barrigão copper deposit: Tennantite-tetrahedrite for thermoelectric and high-technology applications. In *Extended Abstracts Boock of the XII Congresso Ibérico de Geoquímica and XX Semana da Geoquímica, Évora, Portugal, 22–26 September 2019*; Nogueira, P., Moreira, N., Roseiro, J., Maia, M., Eds.; University of Évora: Évora, Portugal, 2019; pp. 255–258. ISBN 978-972-778-121-8.
38. Tabelin, C.B.; Corpuz, R.D.; Igarashi, T.; Villacorte-Tabelin, M.; Ito, M.; Hiroyoshi, N. Hematite-catalysed scorodite formation as a novel arsenic immobilisation strategy under ambient conditions. *Chemosphere* **2019**, *233*, 946–953. [CrossRef] [PubMed]
39. Warr, L.N. IMA–CNMNC approved mineral symbols. *Mineral. Mag.* **2021**, *85*, 291–320. [CrossRef]
40. Moreira, B.; Figueiras, J.; Mateus, A.; Rodrigues, P.; Jorge, R.; Gonçalves, L. A new manganese mineralisation type in the Iberian Pyrite Belt? In *Abstract Book of the X Congresso Ibérico de Geoquímica—XVIII Semana de Geoquímica, Lisbon, Portugal, 19–23 October 2015*; LNEG, Eds.: Lisbon, Portugal, 2015; pp. 133–136, ISBN 978-989-675-039-8. Available online: https://www.researchgate.net/publication/320945506 (accessed on 10 December 2024).